# The influence of a compatibilizer on the thermal and dynamic mechanical properties of PEEK/carbon nanotube composites

Díez-Pascual, A. M.; Naffakh, M.; Gómez, M. A.; Marco, C.; Ellis, G.; González-Domínguez, J. M.; Ansón, A; Martínez, M. T.; Martínez-Rubi, Y.; Simard, B.; Ashrafi, B.



**Publisher's version / Version de l'éditeur:**
https://doi.org/10.1088/0957-4484/20/31/315707
*Nanotechnology, 20, 31, 2009-07-14*

The influence of a compatibilizer on the thermal and dynamic mechanical properties of PEEK/carbon nanotube composites



2009 Nanotechnology 20 315707

(http://iopscience.iop.org/0957-4484/20/31/315707)

Nanotechnology **20** (2009) 315707 (13pp) doi:10.1088/0957-4484/20/31/315707

# The influence of a compatibilizer on the thermal and dynamic mechanical properties of PEEK/carbon nanotube composites

**A M Díez-Pascual[1,5], M Naffakh[1], M A Gómez[1], C Marco[1], G Ellis[1], J M González-Domínguez[2], A Ansón[2], M T Martínez[2], Y Martínez-Rubi[3], B Simard[3] and B Ashrafi[4]**

[1] Departamento de Física e Ingeniería de Polímeros, Instituto de Ciencia y Tecnología de Polímeros, CSIC, c/Juan de la Cierva 3, 28006 Madrid, Spain
[2] Instituto de Carboquímica, CSIC, c/Miguel Luesma Castan 4, 50018 Zaragoza, Spain
[3] Steacie Institute for Molecular Sciences, NRC, 100 Sussex Drive, Ottawa, Canada
[4] Institute for Aerospace Research, NRC, 1200 Montreal Road, Ottawa, Canada

E-mail: adiez@ictp.csic.es

Received 4 March 2009, in final form 5 June 2009
Published 14 July 2009
Online at stacks.iop.org/Nano/20/315707

**Abstract**
The effect of polyetherimide (PEI) as a compatibilizing agent on the morphology, thermal, electrical and dynamic mechanical properties of poly(ether ether ketone) (PEEK)/single-walled carbon nanotube (SWCNT) nanocomposites, has been investigated for different CNT loadings. After a pre-processing step based on ball milling and pre-mixing under mechanical treatment in ethanol, the samples were prepared by melt extrusion. A more homogeneous distribution of the CNTs throughout the matrix is found for composites containing PEI, as revealed by scanning electron microscopy. Thermogravimetric analysis demonstrates an increase in the matrix degradation temperatures under dry air and nitrogen atmospheres with the addition of SWCNTs; the level of thermal stability of these nanocomposites is maintained when PEI is incorporated. Both differential scanning calorimetry and synchrotron x-ray scattering studies indicate a slight decrease in the crystallization temperatures of the compatibilized samples, and suggest the existence of reorganization phenomena during the heating, which are favoured in the composites incorporating the compatibilizer, due to their smaller crystal size. Dynamic mechanical studies show an increase in the glass transition temperature of the nanocomposites upon the addition of PEI. Furthermore, the presence of PEI causes an enhancement in the storage modulus, and hence in the rigidity of these systems, attributed to an improved interfacial adhesion between the reinforcement and the matrix. The electrical and thermal conductivities of these composites decrease with the incorporation of PEI. Overall, the compatibilized samples exhibit improved properties and are promising for their use in industrial applications.

(Some figures in this article are in colour only in the electronic version)

## 1. Introduction

Recently the fabrication of polymer nanocomposites by incorporating nanoscaled carbon fillers into the polymer matrix has become a key technology for advanced composite materials [1, 2]. These nanocomposites, easily processed due to the small diameter of the carbon nanotubes (CNTs), exhibit unique physical properties, such as enhanced tensile strength [3] and exceptionally high electrical and thermal conductivity [4, 5]. This behaviour, combined with their

[5] Author to whom any correspondence should be addressed.

 

low density, makes them suitable for a wide range of commercial and industrial applications, especially for the aerospace industry [6], where the reduction of weight is crucial in order to minimize fuel consumption. However, because of the high cost and limited availability of CNTs, to date only a few practical applications in the industrial field, such as microelectronic devices [7], have evolved. Nowadays, one of the main challenges in aircraft research and technology is the development of cost-effective techniques for manufacturing nanocomposites on a large scale, so that they can be used in structural components, such as wing panels, horizontal and vertical stabilizers, landing gear doors and some sections of the fuselage [8]. Fundamental work in processing, characterization, and analysis/modelling is required before the structural and functional properties of this new class of composites can be optimized. Nevertheless, to make such high performance nanocomposites, a homogeneous distribution of the CNTs inside the polymer matrix, free from agglomerates or entanglements, as well as strong nanotube–resin interface adhesion must be achieved in order to attain efficient load transfer from the matrix to the CNTs.

In the literature, several methods for the preparation of polymer/CNT composites have been reported, including solution mixing [9], sonication [10], melt compounding [11] and *in situ* polymerization [12]. The melt blending approach presents two main advantages: firstly, it is environmentally sound, due to the absence of organic solvents; secondly, it is compatible with conventional industrial processes, such as extrusion, injection and blow moulding; thus being easily implementable. However, generally it is difficult to achieve a homogeneous dispersion of CNTs by this procedure. To improve their distribution throughout the matrix, nanotubes have been purified, ball milled [13], functionalized [14], surface treated with plasma [2] and dispersed in compatibilizing agents [15, 16]. Generally, compatibilizers are block or graft copolymers, chemically identical to, or having affinity with, the matrix, which possesses segments capable of interaction with each blend component. Acting as polymeric surfactants, also called emulsifiers or interfacial modifiers [17], these reduce the interfacial tension, thus promoting interfacial adhesion between the matrix and the dispersed phase. In some cases, the emulsifying ability of the compatibilizer also leads to a reduction of the polydispersity of the filler particle size [18]. Better dispersion and adhesion result in improved mechanical properties of these blends.

In this study, a semicrystalline thermoplastic polymer, poly(ether ether ketone) (PEEK) has been chosen as the polymer matrix due to its excellent thermal and chemical stability [19], and processability suitable for applications in the automobile and aerospace industries. To improve the disentanglement and disaggregation of the CNTs, and their integration inside the matrix, SWCNTs were dispersed in polyetherimide (PEI), an amorphous polymer that is miscible with [20, 21] and structurally similar to PEEK. It has been employed as a compatibilizer due to its high hydrophobic character, commercial availability and chemical compatibility with both components of the composite. In addition, it presents excellent mechanical properties, even at elevated temperature, and exceptional thermooxidative stability [22]. Over the last decade, several papers related to the morphological [20] and thermal [21, 23, 24] characterization of PEEK/PEI mixtures have been published. Furthermore, some studies dealing with PEI-based composites have been recently reported, the most relevant being those published by Rath *et al* [25, 26], where the compatibilizing effect of a third component on liquid crystal polymer/PEI blends has been investigated. Nevertheless, to our knowledge, there is no scientific work to date that employs PEI as a compatibilizer for polymer/SWCNT composites.

The work reported in this manuscript was aimed at studying the efficiency of PEI as compatibilizing agent for PEEK/SWCNT nanocomposites. To investigate its effects, similar specimens, at the same CNT loading, with and without compatibilizer, have been prepared by melt blending after a pre-mixing stage in an organic solvent. An extensive comparative characterization has been carried out in order to evaluate the potential improvement in the filler dispersion induced by the addition of PEI, and the subsequent variations in the thermal, electrical and dynamic mechanical properties of the resulting composite materials.

## 2. Experimental details

### *2.1. Materials*

The matrix used was a commercially available semicrystalline poly(ether ether ketone), PEEK 150P, supplied by Victrex plc, UK ($M_w \sim 40\,000$ g mol$^{-1}$, $T_g = 147\,^{\circ}$C, $T_m = 345\,^{\circ}$C). This low viscosity grade is the most suitable for potential aircraft applications. The polymer, provided as a coarse powder, was vacuum dried at 120 °C for 4 h, and stored in a dry environment before blending. Arc grown SWCNTs were synthesized at the Institute of Carbon Chemistry (ICB-CSIC), Zaragoza, Spain, using a Ni/Y $\sim$ 2/0.5 atomic ratio as the catalyst, according to the procedure reported elsewhere [27]. In order to decrease the metal catalyst content ($\sim$13 wt% Ni, Y) and to remove amorphous carbon particles, these arc grown SWCNTs were treated in a reflux of $HNO_3$ 1.5 M, at 150 °C for 2 h, and then centrifuged at 10 000 rpm for 4 h. This process reduced their metal content by approximately 75%, which demonstrates the effectiveness of the purification step. During the treatment, oxygenated groups are formed which increase the reactivity of the CNTs and therefore improve the anchoring of compatibilizers and their adhesion to the polymer matrix. Laser grown SWCNTs were prepared at the Steacie Institute for Molecular Sciences (SIMS-NRC), Canada. The residual catalyst (Ni, Co) was lower than 4 wt%, and they were used without further purification. The compatibilizing agent, polyetherimide, PEI 250G, was provided by Sigma-Aldrich in a pellet form ($M_w \sim 30\,000$ g mol$^{-1}$, $T_g = 217\,^{\circ}$C, $d_{25\,^{\circ}C} = 1.27$ g cm$^{-3}$). PEI is an amorphous, transparent and amber coloured high performance thermoplastic, with functional groups compatible with both the CNTs and the matrix. The SWCNTs were wrapped with PEI in liquid media: 25 mL of a PEI chloroform solution (1.5% w/w) was mixed with $\sim$370 mg of SWCNTs (either laser as grown or acid

**Table 1.** Characteristics and nomenclature of the SWCNTs used for the preparation of the composites. (Note: The compatibilizing agent (PEI) and metal content were determined from TGA thermograms. $T_{mr}$ corresponds to the temperature of the maximum rate of weight loss under a dry air atmosphere. $D$ is the average bundle diameter obtained from SEM micrographs.)

| Preparation method | Compat. (wt%) | Metal (wt%) | $T_{mr}$ (°C) | $D$ (nm) | Sample code |
|---|---|---|---|---|---|
| Laser (as grown) | — | 3.9 | 493 | 39.8 | LC1m |
| Arc (purified) | — | 3.2 | 541 | 20.4 | ZC1p |
| Laser (PEI dispersed) | 6.9 | 4.1 | 488 | 33.6 | LC1 + PEI |
| Arc (PEI dispersed) | 8.3 | 3.3 | 532 | 19.9 | ZC1 + PEI |

treated arc discharge) with intense stirring for 5 min. Each mixture was treated with a Hielscher DRH-UP400S ultrasonic tip (400 W maximum power; 24 kHz maximum frequency) for 60 min at 50% oscillation amplitude and 50% cycle time. The resulting dispersion was observed to be highly stable. Subsequently, it was filtered using a 0.2 $\mu$m pore size PTFE membrane and dried under vacuum at 60 °C for 2 h to assure total evaporation of the solvent. In order to homogenize the particle size, the resulting solid was milled in an agate mortar.

Before proceeding to the preparation of the composites, an extensive characterization of the different SWCNTs used was carried out. A high degree of agglomeration and a non-homogeneous size distribution of the diameters was observed from their SEM images. As expected, the average bundle diameter decreased in the presence of the compatibilizer. Thermogravimetric analysis (TGA) under dry air conditions revealed the temperatures of the maximum oxidation rates ranging between 488 °C for laser grown SWCNTs dispersed in PEI to 541 °C for the purified SWCNTs. Furthermore, the comparison of the decomposition curves of SWCNTs with and without compatibilizer, together with the thermogram of pure PEI, allowed the calculation of the composition of the mixtures SWCNT + PEI employed for the preparation of the nanocomposites. These parameters are summarized in table 1, which also includes the sample nomenclature employed throughout the text.

### 2.2. Preparation of PEEK/SWCNT composites

To improve the distribution of the CNTs in the matrix, nanocomposites containing concentrations of 0.1, 0.5 and 1 wt% SWCNTs were prepared following a procedure based on the use of mechanical treatment in alcohol. Firstly, PEEK was ground with a ball mill in order to reduce its particle size. Secondly, the polymer was mixed with the different types of SWCNT (see table 1). Then, each mixture was dispersed in 30 ml of ethanol and sonicated in an ultrasonic bath for 30 min. Subsequently, the dispersion was dried under vacuum (70 mbar) at 50 °C for 5 min, sonicated for another 30 min, and heated in an oven until the ethanol was completely eliminated.

The melt compounding was performed in a Thermo-Haake MiniLab micro-extruder, at 380 °C, using 5 g of material in total, with a rotor speed of 150 rpm. Mixing times of 20 min were applied, selected as the standard conditions derived from preliminary tests. For comparative purposes, a reference PEEK/PEI blend containing the same amount of compatibilizer as the PEEK/SWCNT (1 wt%) nanocomposites was also prepared following the aforementioned process. Homogeneous films, prepared in a Collin press at 380 °C under 130 bar and cooled between aluminium plates at 15 °C, were used for the different characterizations.

### 2.3. Thermogravimetric analysis

The thermal stability of the SWCNTs and nanocomposites was analysed by thermogravimetric analysis (TGA). The measurements were carried out using a TA-Q500 thermobalance, at a heating rate of 10 °C min$^{-1}$, under both inert (nitrogen) and oxidizing (dry air) atmospheres. The analysis was performed on samples with an average mass of 10 mg, under dynamic conditions, from room temperature to 900 °C, with a gas purge rate of 150 mL min$^{-1}$. The following characteristic degradation temperatures were selected: $T_i$, the initial degradation temperature; $T_{10}$, temperature for 10% weight loss; $T_{mr}$, temperature of maximum rate of weight loss.

### 2.4. Differential scanning calorimetry

The crystallization and melting behaviour of the nanocomposites were investigated by DSC using a Mettler TA 400/DSC 30 differential scanning calorimeter, operating under a nitrogen flow. Samples of approximately 10 mg were weighed and sealed in aluminium sample pans. Before the heating and cooling scans, the composites were melted at 380 °C and maintained at this temperature for 5 min in order to erase the thermal history of the material. Subsequently they were cooled from 380 to 30 °C at a rate of 10 °C min$^{-1}$, and then heated from 30 to 380 °C at 10 °C min$^{-1}$.

The transition temperatures were taken as the peak maxima or minima in the calorimetric curves, and the apparent enthalpies were calculated as normalized integrals of the corresponding peaks. The levels of crystallinity of PEEK in the nanocomposites were determined using the following relation: $(1-\lambda)_m = \Delta H_{m,PEEK}/(\Delta H^{\circ}_{m,PEEK} \times w_{PEEK})$, where $\Delta H_{m,PEEK}$ is the apparent melting enthalpy of PEEK, $w_{PEEK}$ is the weight fraction of PEEK and $\Delta H^{\circ}_{m,PEEK}$ is the extrapolated value of the enthalpy corresponding to the melting of a 100% crystalline sample, taken as 130 J g$^{-1}$ [28].

### 2.5. X-ray diffraction

Small and wide-angle x-ray scattering (SAXS/WAXS) experiments were performed using synchrotron radiation at the A2 beamline of the HASYLAB synchrotron (DESY, Hamburg). A description of the instrumentation can be found elsewhere [29]. The beam was monochromatized by Bragg reflection through a germanium single crystal ($\lambda$ = 0.15 nm). Linear Gabriel detectors were used to collect the scattered light. The sample to detector distance for SAXS was 236 cm, and for WAXS was 135 mm, allowing diffractograms to be registered in the angular range of $2\theta$ = 10°–34°. The scattering angle of the SAXS pattern was calibrated with RTT (rat tail tendon), and that of the WAXS profile was calibrated with a PET standard. To ensure adequate

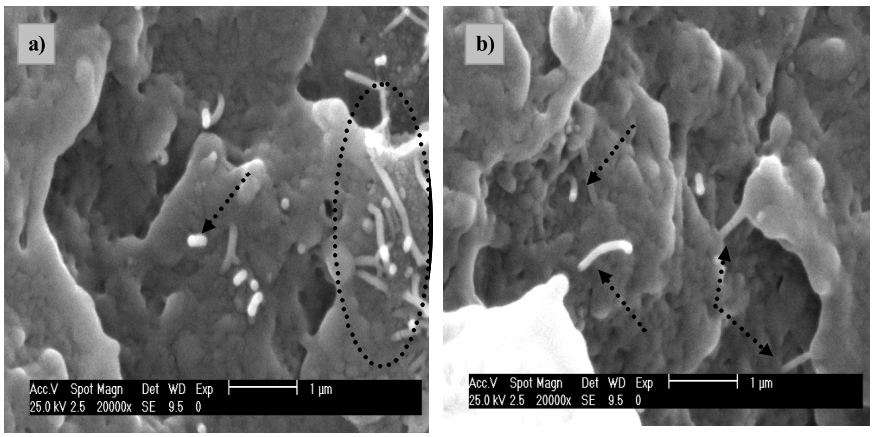


**Figure 1.** Typical SEM micrographs from fractured surfaces of PEEK/SWCNT (1 wt%) nanocomposites at a magnification of 2000×: (a) PEEK/LC1m; (b) PEEK/LC1 + PEI. The arrows indicate randomly distributed nanotube bundles in the matrix. The circle shows a small region of agglomerated CNT in the non-compatibilized sample.

temperature control, samples covered by aluminium paper were thermostated inside a vacuum system. The methodology used in the isothermal crystallization and melting experiments of the nanocomposites was similar to that described for the calorimetric measurements. Diffractograms were recorded with an acquisition time of 30 s (wait time = 20 s and read time = 10 s), employing a total cycle time of 35 min.

WAXS measurements at 25 °C were also performed in a D8 Advanced Bruker Instrument, equipped with a Göbel mirror and a Vantec PSD detector, with a voltage of 40 kV and an intensity of 40 mA, using Cu K$\alpha$ ($\lambda = 0.154\,18$ nm) radiation, with an aperture of 0.6 mm. Diffractograms were registered on films or powder, in the angular region of $2\theta$ = 5°–40°, at room temperature, with a scan speed of 0.2 s and angular increment of 0.02°.

### *2.6. Scanning electron microscopy*

The dispersion of the SWCNTs in the matrix was characterized using a Philips XL 30 ESEM scanning electron microscope (SEM), with a voltage of 25 kV and an intensity of $9 \times 10^{-9}$ A. The nanocomposite film samples were fractured in liquid nitrogen and then heated in an oven for 3 h at 200 °C to improve the visibility of the CNTs. In order to avoid charging during electron irradiation, the specimens were covered with an approximately 5 nm overlayer of an Au–Pd (80–20) alloy in Balzers SDC 004 evaporator, using a evaporation time of 242 s at 20 mA.

### *2.7. Dynamic mechanical analysis*

The dynamic mechanical properties of the composites were studied using a Mettler DMA 861 dynamic mechanical analyzer. Rectangular shaped samples of $\sim 19.5 \times 4 \times 0.5$ mm$^3$ were mounted in a large tension clamp. The measurements were performed in the tensile mode at frequencies of 0.1, 1 and 10 Hz, in the temperature range between −130 and 260 °C, at a heating rate of 2 °C min$^{-1}$. A dynamic force of 6 N was used, oscillating at fixed frequency and with an amplitude of 30 $\mu$m.

### *2.8. Electrical and thermal conductivity*

Room temperature DC volume conductivity measurements were performed on thin film samples (approx. 0.5 mm thick and 3 cm diameter) using a DC power supply (Global Specialties 1302) applying a constant voltage, and an analogue multimeter (Keithley 2010) to measure the current. The applied voltage was measured with a digital multimeter (Newport HHM290). Silver conductive epoxy paint electrodes were applied over the whole sample surface to guarantee well-aligned electrodes of exactly the same size.

The thermal conductivity of the films was characterized with a THASYS Hukseflux thermal sensor equipped with a thin heater apparatus (THA01) and a measurement and control unit (MCU). The samples were immersed in glycerol to eliminate the problem of contact resistance. The thermal conductivities were determined by measuring the heat flux and the differential temperature across the samples. At least 3 specimens for each composition were tested and the average value taken.

## 3. Results and discussion

### *3.1. Carbon nanotube dispersion in the nanocomposites*

Scanning electron microscopy (SEM) was used to observe the surface morphology of the cryofractured films and qualitatively visualize the state of dispersion of the carbon nanotubes in the polymer matrix. Achieving a good distribution of the organic filler is commonly a difficult task, because carbon nanotubes have a strong tendency to gather and form bundles [30], as evidenced by SWCNT SEM analysis. Figure 1 compares typical micrographs of PEEK/LC1m (a) and PEEK/LC1 + PEI (b) nanocomposites, both containing 1 wt% SWCNT loading; similar images were obtained from samples prepared with arc-purified SWCNTs. The former composite shows a less homogeneous distribution of the CNTs, which appear as bright spots; the size of the domains of the dispersed phase is relatively larger and there are small regions where CNT agglomeration can be observed (see the circle marked

on the image). However, the interfacial adhesion between the two phases seems to be good, as no open ring holes are found around the nanotubes. The compatibilized sample (figure 1(b)) displays a random and improved dispersion of the reinforcing phase; addition of the compatibilizer induced CNT disentanglement and disaggregation inside the polymer matrix, leading to a reduction of the organic filler domains. No agglomerates or entanglements were observed in the examined areas, which results in a larger effective contact area and thus stronger CNT–PEEK interfacial adhesion, reflected in the more efficient load transfer under stress conditions. We have also found that the improvement in the degree of dispersion of the reinforcement for the compatibilized samples is less significant at lower CNT loading, as the tendency to form agglomerates increases when the concentration rises.

### *3.2. Thermal stability*

The influence of the compatibilizing agent on the thermal stability of the nanocomposites has been investigated by thermogravimetric experiments, carried out under both inert and oxidative conditions, from 100 to 900 °C. The degradation curves of composites containing 1 wt% SWCNT are presented in figure 2. For comparison purposes, the TGA profiles of the pure compounds and the reference PEEK/PEI mixture are also included in the plot. It is clear from figure 2(a) that under an inert atmosphere all the samples present a single decomposition step, with approximately 45% weight loss at 650 °C. The degradation of pure PEEK has an initiation temperature ($T_i$) of about 520 °C, and shows the maximum decomposition temperature ($T_{mr}$) at 558 °C. The addition of 1 wt% SWCNT enhances the thermal stability of the matrix: $T_i$ and $T_{max}$ are increased by an average of 25 and 20 °C, respectively. The comparison between the decomposition curves of compatibilized and non-compatibilized nanocomposites (see figure 2(a)) reveals that the incorporation of PEI slightly decreases the degradation temperatures of the nanocomposites. This fact could be explained by considering that the compatibilizing agent has lower thermal stability than the matrix ($T_{i-PEI}$ = 502 °C, $T_{mr-PEI}$ = 535 °C). Nevertheless, the reference mixture presents a similar degradation curve to the matrix, albeit shifted towards lower temperatures by ∼4 °C. Therefore, the aforementioned destabilization may be also attributed to small changes in the interfacial interactions between the CNTs and the matrix due to the presence of the compatibilizer.

The thermal stability of the nanocomposites is strongly influenced by the type of atmosphere. As observed in figure 2(b), the degradation of these composites in dry air takes place in two consecutive stages, and the major weight loss (about 62–65% for all samples) occurs in the second step, which leads to the total decomposition of the material. PEEK begins to decompose at 472 °C, about 50 °C lower than in a nitrogen atmosphere, and the two maximum degradation rates ($T_{max\,I}$ and $T_{max\,II}$) appear at 530 and 592 °C, respectively. The incorporation of SWCNTs shifts the matrix curve towards higher temperatures, this stabilization effect being qualitatively similar to that observed under an inert

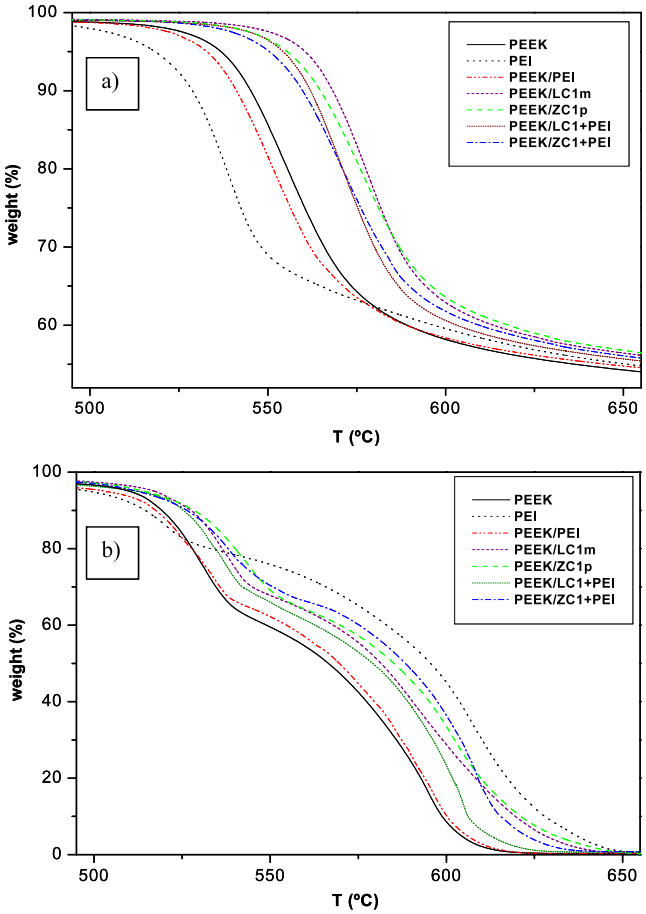


**Figure 2.** TGA curves between 500 and 650 °C for the pure compounds and different types of PEEK/SWCNT (1 wt%) nanocomposites, at a heating rate of 10 °C $min^{-1}$ (a) in a nitrogen atmosphere and (b) in a dry air atmosphere.

environment. Compatibilized systems present a lower initial degradation temperature: $T_i$ is decreased by an average of 5 °C with respect to nanocomposites without the compatibilizer. However, the compatibilizing agent does not significatively modify $T_{max\,I}$ or $T_{max\,II}$. To understand the aforementioned phenomena, the degradation curves of PEI and PEEK/PEI samples must be considered; these are displayed in figure 2(b). The thermal oxidation of the amorphous polymer is also a two-step process, which starts at around 6 °C below that of the matrix. $T_{max\,I}$ appears about 10 °C lower, whereas the second stage is shifted towards higher temperatures, and $T_{max\,II}$ increases around 20 °C. On the other hand, the TGA curve of the reference sample resembles that of PEEK, with maximum degradation rates taking place at approximately the same temperatures. This is in agreement with the fact that the compatibilizing agent maintains the levels of thermal stability obtained by the incorporation of the CNTs. Similar observations have been found in other studies focused on the influence of copolymer compatibilizers on the thermal properties of blends [31, 32].

Regarding the influence of the type of SWCNT, it is clear that composites containing purified SWCNTs exhibit higher degradation temperatures. This is consistent with the results

**Table 2.** Characteristic temperatures of the PEEK/SWCNT nanocomposites obtained from TGA. (Note: The displayed temperatures are: $T_i$: initial degradation temperature obtained at 2% weight loss; $T_{10}$: temperature for 10% weight loss; $T_{mr}$: temperature(s) of maximum rate of weight loss, determined from the peaks of the first derivative of the TGA curve (see the explanation in the text).)

| | Nitrogen | | | Dry air | | |
|---|---|---|---|---|---|---|
| Mat. (% SWCNT) | $T_i$ (°C) | $T_{10}$ (°C) | $T_{mr}$ (°C) | $T_i$ (°C) | $T_{10}$ (°C) | $T_{mr}$ (°C) I, II |
| PEEK | 521 | 544 | 558 | 472 | 520 | 530, 592 |
| PEEK/LC1m (0.1) | 542 | 557 | 565 | 480 | 524 | 534, 596 |
| PEEK/LC1m (0.5) | 544 | 563 | 573 | 483 | 526 | 538, 600 |
| PEEK/LC1m (1.0) | 546 | 568 | 577 | 484 | 529 | 541, 603 |
| PEEK/ZC1p (0.1) | 536 | 550 | 564 | 481 | 523 | 537, 597 |
| PEEK/ZC1p (0.5) | 540 | 558 | 574 | 483 | 527 | 542, 602 |
| PEEK/ZC1p (1.0) | 543 | 564 | 578 | 485 | 531 | 545, 606 |
| PEI | 502 | 522 | 535 | 467 | 516 | 520, 613 |
| PEEK/PEI | 518 | 541 | 554 | 470 | 519 | 529, 594 |
| PEEK/LC1 + PEI (0.5) | 537 | 556 | 569 | 475 | 524 | 535, 599 |
| PEEK/LC1 + PEI (1.0) | 541 | 562 | 572 | 478 | 527 | 539, 605 |
| PEEK/ZC1 + PEI (0.1) | 535 | 549 | 562 | 476 | 523 | 536, 598 |
| PEEK/ZC1 + PEI (0.5) | 537 | 553 | 571 | 479 | 525 | 540, 604 |
| PEEK/ZC1 + PEI (1.0) | 539 | 558 | 574 | 481 | 529 | 543, 609 |

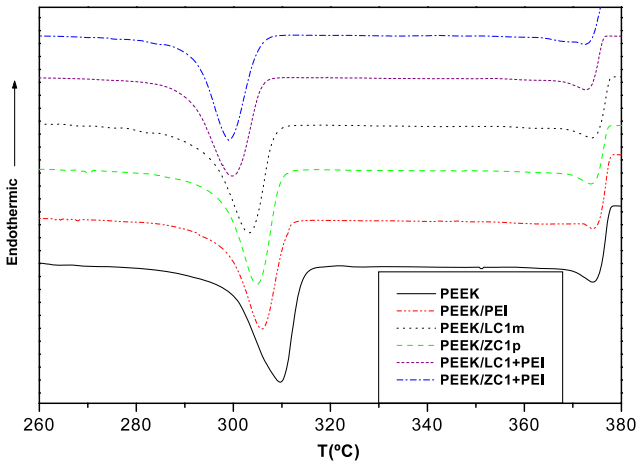


**Figure 3.** DSC crystallization thermograms between 260 and 380 °C of PEEK/SWCNT (1 wt%) nanocomposites at rate of 10 °C $min^{-1}$.

obtained from the TGA study of the SWCNTs (see table 1), which shows that these nanotubes are more resistant to the oxidation process, probably due to a lower content of metal impurities that might catalyze its decomposition [33].

The effect of SWCNT content on the thermal behaviour of the nanocomposites can be seen from table 2, which summarizes the values of the characteristic temperatures for all the PEEK/SWCNT systems. No significant differences between compatibilized and non-compatibilized composite series are observed. The incorporation of an increasing CNT content progressively enhances the stability of PEEK. This stabilization can be attributed to the barrier effect of the SWCNTs, which hinders the diffusion of the degradation products from the bulk of the polymer to the vapour phase [34].

### *3.3. Crystallization behaviour*

From a technological point of view, the dynamic crystallization of blends and composites is of a great interest, because most processing routes take place under these conditions. To evaluate the possible influence of the compatibilizer on the crystallization behaviour of the polymer matrix in the composite, different kinds of PEEK/SWCNT nanocomposites, with a varying concentration of CNTs, were subjected to DSC analysis under non-isothermal conditions. The cooling thermograms for samples containing 1 wt% SWCNT are shown in figure 3. It can be observed that the crystallization temperature ($T_c$) is 309 °C for pure PEEK, and around 304 °C for composites without compatibilizer. The incorporation of SWCNTs dispersed in PEI leads to a significant shift of the crystallization peak towards lower temperatures, decreasing the PEEK $T_c$ by nearly 10 °C. However, the apparent crystallization enthalpy $\Delta H_{cr}$ remains almost unchanged by the addition of CNTs with or without compatibilizer, which results in small differences between the levels of crystallinity of the samples; lower than 5%. To understand these results, different facts must be considered in these systems. Firstly, nanoconfinement [35] and multiple nucleation effects: although CNTs provide heterogeneous nucleation sites for PEEK crystallization, the formation of a well-developed nanotube network imposes important restrictions on polymer chain diffusion and crystal growth, which slows down the overall crystallization process, leading to lower $T_c$ values for the nanocomposites. A similar behaviour in the retardation of the crystal growth, arising from the effect of stiff nanotubes on the overall mobility in the blend, has been recently reported for PEO/MWNT composites [36]. Furthermore, a detailed crystallization study of PPS/IF-$WS_2$ nanocomposites [37] revealed a reduction of the matrix crystallization rate for very low concentrations of nanoparticles, attributed to a higher fold surface free energy of the polymer chains. Secondly, the influence of the compatibilizer itself on the PEEK crystallization process must be analysed. To clarify this effect, the PEEK/PEI reference sample was also studied by DSC (see figure 3). The $T_c$ of PEEK was lowered by 4 °C, which can be easily understood taking into account that PEI is an amorphous polymer miscible with the matrix which perturbs

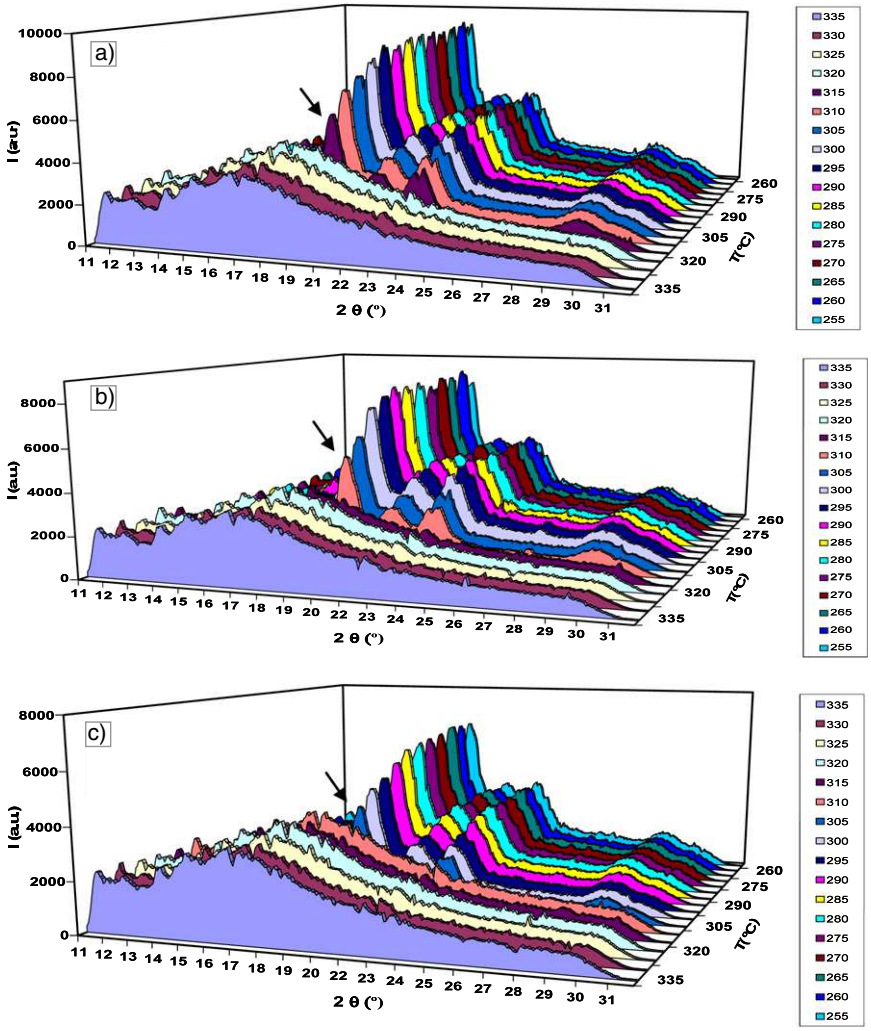


**Figure 4.** WAXS diffractograms of (a) PEEK, (b) PEEK/LC1m (1 wt%) and (c) PEEK/LC1 + PEI (1 wt%), obtained during cooling from the melt to room temperature at 10 °C min$^{-1}$. The arrow indicates the temperature corresponding to the appearance of the crystalline reflections.

the crystallization of PEEK. This is a common attribute of miscible and compatible blends containing one non-crystallizing polymer [24, 38], and the most likely explanation is the reduction in chain mobility imposed by the strong interactions between the components that take place between the oxygen ion-pair electrons of the ether group in PEEK and the electron-deficient imide rings in PEI. Moreover, our results are in good agreement with previous PEEK/PEI DSC studies, where a decrease of PEEK crystallization rate was found upon increasing PEI content [21, 23]. Hence, two synergic effects seem to be the origin of the remarkable decrease in the $T_c$ of the compatibilized nanocomposites: the nanoconfinement effect and the incorporation of small amounts of an amorphous polymer that moderately hinders PEEK crystallization.

The aforementioned effects of the compatibilizing agent have been also found at lower SWCNT content, as observed in table 3, which presents experimental DSC data and the degree of crystallinity of all the nanocomposites prepared. For the same CNT loading, samples including PEI show the lowest $T_c$ values. With increasing CNT concentration, the effects became stronger, and the $T_c$ decrease is more pronounced. However, no remarkable differences are observed within the crystallization parameters of composites incorporating SWCNTs synthesized by different methods.

### *3.4. Crystalline structure*

To verify that the incorporation of the compatibilizer delays the crystallization of the matrix, and to obtain information about its possible influence on the crystalline structure of PEEK, we have monitored the melting and crystallization processes by real time simultaneous SAXS and WAXS experiments, using synchrotron radiation. Figure 4 presents, as an example, the WAXS diffractograms of pure PEEK (a), PEEK/LC1m (b) and PEEK/LC1 + PEI (c) nanocomposites, at 1 wt% SWCNT content, recorded during cooling from the melt to room temperature, at a rate of 10 °C min$^{-1}$. Four main Bragg reflections can be observed at $2\theta$ angles of 18.7°, 20.6°, 22.8° and 28.8°, which correspond to the diffraction of the (110), (111), (200) and (211) crystalline planes [39] of the orthorhombic unit cell, respectively. The appearance of peaks in WAXS patterns takes place when the material

**Table 3.** DSC crystallization and melting data of PEEK/SWCNT nanocomposites. (Note: The displayed data are: $T_c$: crystallization temperature; $\Delta H_{cr}$: apparent crystallization enthalpy; $T_m$: melting temperature; $\Delta H_{mr}$: apparent melting enthalpy; $(1-\lambda)_c$ and $(1-\lambda)_m$: crystallization and melting crystallinities, derived from the peak areas.)

| Mat. (% SWCNT) | $T_c$ (°C) | $\Delta H_{cr}$ (J g$^{-1}$) | $(1-\lambda)_c$ (%) | $T_m$ (°C) | $\Delta H_{mr}$ (J g$^{-1}$) | $(1-\lambda)_m$ (%) |
|---|---|---|---|---|---|---|
| PEEK | 309.1 | 55.3 | 42.5 | 344.2 | 58.2 | 44.8 |
| PEEK/LC1m (0.1) | 307.5 | 57.8 | 44.5 | 343.5 | 58.5 | 45.0 |
| PEEK/LC1m (0.5) | 305.1 | 56.5 | 43.7 | 343.1 | 57.3 | 44.3 |
| PEEK/LC1m (1.0) | 303.3 | 54.4 | 42.3 | 342.6 | 55.7 | 43.2 |
| PEEK/ZC1p (0.1) | 308.1 | 58.2 | 44.8 | 343.9 | 58.6 | 45.0 |
| PEEK/ZC1p (0.5) | 306.6 | 57.0 | 44.1 | 343.2 | 57.5 | 44.4 |
| PEEK/ZC1p (1.0) | 304.3 | 54.6 | 42.4 | 342.6 | 56.6 | 44.0 |
| PEEK/PEI | 305.2 | 53.3 | 41.1 | 343.0 | 55.4 | 42.7 |
| PEEK/LC1 + PEI (0.5) | 303.7 | 54.6 | 42.2 | 342.7 | 56.0 | 43.3 |
| PEEK/LC1 + PEI (1.0) | 299.9 | 52.5 | 40.7 | 341.2 | 55.1 | 42.8 |
| PEEK/ZC1 + PEI (0.1) | 305.9 | 56.0 | 43.0 | 343.0 | 57.2 | 44.0 |
| PEEK/ZC1 + PEI (0.5) | 303.4 | 54.8 | 42.4 | 341.9 | 56.1 | 43.4 |
| PEEK/ZC1 + PEI (1.0) | 299.5 | 52.7 | 40.9 | 340.3 | 54.9 | 42.6 |

attains an appreciable degree of crystallinity. According to the diffractograms, the crystallization of pure PEEK initiates at around 315 °C, showing an increase of the peak intensities up to ∼295 °C. This temperature range, which corresponds to the growth of polymer crystals, correlates well with the temperature interval observed for the crystallization peak in the DSC cooling thermograms. For the compatibilized and non-compatibilized composites, the crystalline reflections appear at around 310 and 305 °C, respectively; similar results were obtained for composites including purified arc grown SWCNTs, which confirms once again that the presence of the CNTs, and especially the compatibilizer, delays the crystallization process of PEEK. However, its crystalline structure remains unchanged, as no shift in the position of the Bragg reflections is found.

The degree of crystallinity $X_c$ of the samples was calculated from WAXS diffractograms at 25 °C using the following relation: $X_c = I_c/(I_c + I_a)$, $I_c$ and $I_a$ being the integrated intensities of the crystalline and amorphous phases, respectively. The values obtained for the different nanocomposites are in very good agreement with those derived from DSC thermograms.

### *3.5. Melting behaviour*

Figure 6 shows the DSC heating thermograms obtained after dynamic crystallization for pure PEEK and nanocomposites with a 1 wt% CNT loading. The data derived from all the calorimetric curves are included in table 3. The melting temperature ($T_m$) of pure PEEK is 344.2 °C, and it shifts slightly to lower values (by an average of 2 °C) with the incorporation of un-wrapped SWCNTs. This effect is maximized in composites including compatibilizer, where $T_m$ decreases by approximately 4 °C. These observations are in contrast to the DSC study reported by Shaffer *et al* [40], dealing with vapour grown CNF/PEEK composites prepared by injection moulding, where the melting behaviour of PEEK remained unaffected by the presence of the nanofibres. This contradiction can be explained; based on differences between CNTs and carbon nanofibres (purity, quality, aspect ratio, nature of impurities) and on the processing routes employed for the preparation of the materials. It is also important to notice that a small variation of the specific heat associated with the glass transition of the matrix in the nanocomposites can be seen in the heating thermograms. The compatibilizer shifts this transition towards higher temperatures; this phenomenon will be discussed in detail by DMA measurements.

On the other hand, the analysis of the SAXS diffractograms was performed using the Lorentz correction [41]. The maximum of the plot $Is^2$ versus the scattering vector $s$ ($s = (2/\lambda)\sin\theta$, where $\theta$ is the scattering angle and $\lambda$ the wavelength) was used to calculate the long period $L(L = 1/s_{max})$ as a function of the temperature. $L$ represents the sum of the average thickness of the crystal lamellae and of the interlamellar amorphous regions. Figure 6 presents the $L$ values for pure PEEK and different PEEK/SWCNT nanocomposites, at 1 wt% CNT loading, obtained during heating from room temperature to 360 °C, at a rate of 10 °C min$^{-1}$. A strong increase of the long spacing of PEEK with temperature is found from around 260 °C up to the approach to the melting point. This range approximately corresponds to the increase in the peak intensities observed in the WAXS diffractograms (figure 4). The aforementioned behaviour indicates the existence of reorganization phenomena and improvement (i.e., perfection and thickening) of the PEEK crystals during the heating cycles subsequent to the crystallization process, which have been usually interpreted in terms of melting–recrystallization phenomena or annealing effects on the same crystals [39, 42, 43]. Moreover, it can explain the differences found, over the whole composition range, between the crystallinities obtained from DSC melting and cooling thermograms (see table 3).

The comparison of the long period data for the different samples reveals that, at room temperature, all nanocomposites present lower $L$ values than those of the pure PEEK. This indicates that the melting behaviour of the composites is controlled by the previous crystallization process; the reduction in the crystallization temperature of PEEK leads to the formation of smaller and less perfect crystals. Moreover,

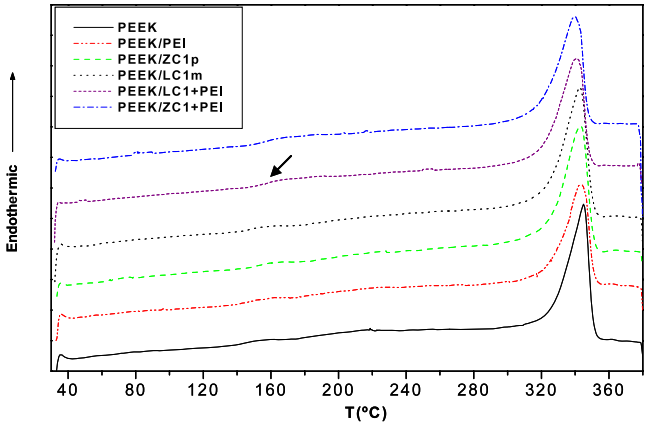


**Figure 5.** DSC melting scans of PEEK/SWCNT (1 wt%) nanocomposites, at a rate of 10 °C min$^{-1}$. The arrow indicates the glass transition of the polymer matrix in the composite.

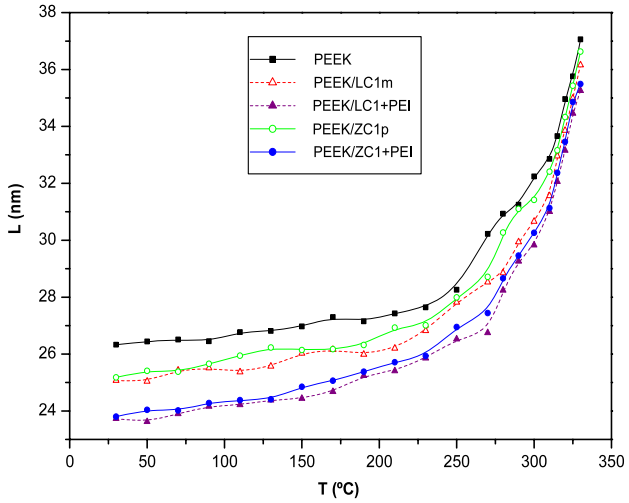


**Figure 6.** Long period (L) values of PEEK/SWCNT (1 wt%) nanocomposites obtained from SAXS diffractograms, during heating from 30 to 360 °C, at a heating rate of 10 °C min$^{-1}$.

the compatibilized samples present the smallest long period data; thus at 30 °C the value of $L$ for the matrix decreases by about 10%. This behaviour is in agreement with the lower crystallization temperature observed from the DSC curves of the compatibilized samples (see figure 3). However, these nanocomposites show a greater increase in the $L$ value during heating, since the effect of reorganization and perfection of the PEEK crystals is favoured in samples with a smaller crystal size. Differences between $L$ values of the composites and the matrix decrease with increasing temperature, and are reduced to approximately 5% in the vicinity of the melting point. This is consistent with the small $T_m$ decrease with respect to that of the matrix observed from the DSC heating curves of the nanocomposites (figure 5). No significant differences are found between the long period values of samples containing laser or arc grown SWCNTs, corresponding to composites with similar crystallization temperatures (see table 3).

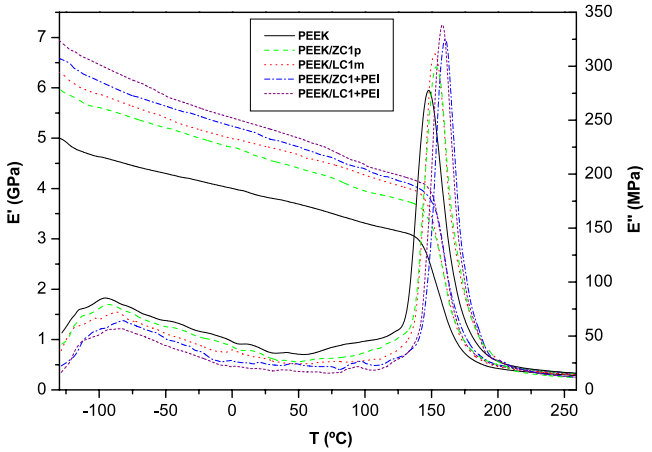


**Figure 7.** Storage modulus $E'$ and loss modulus $E''$ as a function of temperature, for the different types of PEEK/SWCNT (1 wt%) nanocomposites, obtained from DMA measurements at a frequency of 1 Hz.

### *3.6. Dynamic mechanical properties*

The main goal of compatibilization is to improve the mechanical properties of the composites which determine the use of the material. These properties depend on many factors, including the size and degree of dispersion of the filler and the adhesion at the CNTs–matrix interface. In this study, the effect of the compatibilizer on the mechanical response of the nanocomposites has been explored by DMA. Figure 7 shows the development of the storage modulus ($E'$) and loss modulus ($E''$) as a function of temperature, for pure PEEK and several nanocomposites including a 1 wt% SWCNT loading, at a frequency of 1 Hz. As can be observed, $E'$ decreases slowly and progressively with temperature, showing a very strong decay (higher than 85%) in the temperature range between 140 and 180 °C, which corresponds to the glass transition of the material. This fall in the modulus is attributed to an energy dissipation phenomenon involving cooperative motions of the polymer chains [44]. It is evident that the incorporation of CNTs induces a remarkable increase in the storage modulus of the matrix at temperatures below the glass transition, which becomes worthless at higher temperatures. The increase in $E'$ is more pronounced for the composites incorporating PEI, since these correspond to samples with an improved CNT dispersion, according to the SEM micrographs. Thus, at room temperature, the compatibilized nanocomposite including laser SWCNTs increases the matrix $E'$ by approximately 35%, whereas this improvement is reduced to ∼27% for the non-compatibilized sample. To understand these results, $E'$ for pure PEI and the PEEK/PEI blend must also be considered, and their values at 25 °C are compared to that of the matrix in figure 8. Although $E'$ of the amorphous polymer is slightly higher than that of PEEK, the increment for the reference mixture is lower than 1%. Therefore, the modulus increase in the compatibilized nanocomposites should be attributed to the improved interfacial adhesion and stress transfer ability between the reinforcement and polymer host interfaces. An analogous improvement of the storage modulus

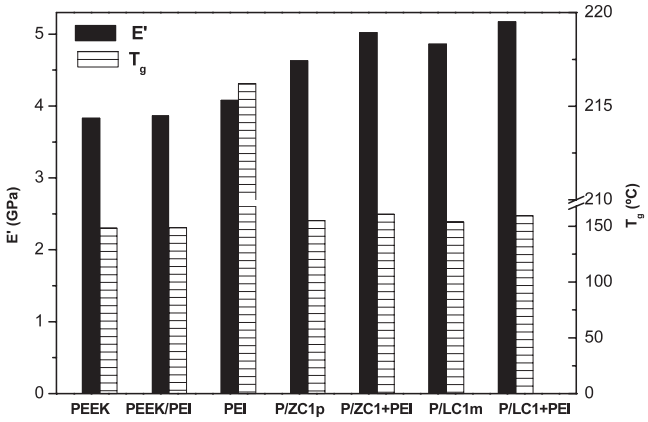


**Figure 8.** Comparison between the storage modulus $E'$, at 25 °C, and the glass transition temperature $T_g$, of the pure compounds and the different types of PEEK/SWCNT (1 wt%) nanocomposites, obtained from DMA measurements at a frequency of 1 Hz. To simplify the nomenclature, P denotes the PEEK matrix.

in compatibilized blends has been described in the literature for ternary PEI-based composites, and explained in terms of the surfactant role of the compatibilizer, which promotes the interfacial adhesion matrix filler and thereby reduces the molecular mobility of the polymer chains [25, 26].

The development of the loss modulus of PEEK as a function of temperature, figure 7, exhibits a low broad peak (centred around −95 °C), attributed to the $\beta$ relaxation [45], associated with local motions of the ketone groups, and an intense sharp peak (at 148.3 °C), denominating the $\alpha$ relaxation [46], whose maximum corresponds to the glass transition temperature ($T_g$) of the polymer. The addition of SWCNTs results in a reduction of the magnitude of $E''$ at temperatures below $T_g$. Furthermore, the $\beta$ relaxation is broadened, smoothed and shifted to higher temperatures. These effects are more pronounced for the composites containing PEI, which suggests that their improved interfacial interactions CNT–PEEK make the movement of the ketone groups more difficult. Goodwin *et al* [47] also found a broadening and a decrease in magnitude for the loss curves of PEEK/PEI blends when compared with the spectra of the pure components, ascribed to concentration fluctuations and the increased range of coupled interactions in the mixture. Moreover, our compatibilized nanocomposites show another small sub-$T_g$ transition at around 100 °C, which probably correlates with the $\beta$ relaxation of pure PEI, related to the movement of the imide groups [47].

Regarding the glass transition, it is clear that the presence of CNTs, which restrict the mobility of the polymer chains, shifts the position of the matrix $\alpha$ peak towards higher temperatures, as evidenced from figure 8, which compares $T_g$ values of the pure compounds and the different nanocomposites. The $T_g$ increase is considerably higher for the compatibilized samples. Thus, the incorporation of 1 wt% ZC1p shifted $T_g$ by about 7 °C, whereas the same amount of these SWCNTs dispersed in PEI raised it by 12 °C. This behaviour could be attributed to the fact that the glass transition in the amorphous polymer takes place at 216.2 °C, approximately 68 °C above that in PEEK. To clarify this influence, the $T_g$ of the PEEK/PEI mixture was accurately determined by DMA as 148.8 °C, in good agreement with theoretical calculations based on the Fox equation for miscible blends [48]. As this value is almost the same as that observed in pure PEEK, the compatibilizing effect seems to be responsible for the significant $T_g$ increase found in composites containing PEI, due to the chain motion restriction induced by the improved adhesion between the matrix and filler phases. On the other hand, the incorporation of the compatibilizer also leads to an increase in the height of the glass transition peak, probably related to the more homogeneous distribution of the CNTs in these nanocomposites, which facilitates heat transport. In contrast to our observations, Rath *et al* [25] found a decrease in the height of the loss modulus peak and a $T_g$ shift towards lower temperatures with the addition of the compatibilizer, caused by an increase in the flexibility of the polymer chains. The discrepancies with our results should be attributed to the nature of the compatibilizing agent and its degree of miscibility with the matrix.

Our experimental data reveal that the influence of the compatibilizer in the DMA behaviour of the composites is repeated at other frequencies, with an increase in both the storage modulus and the transition temperatures as the frequency rises. Focusing on the different types of nanocomposites, over the concentration range studied, improved mechanical properties are systematically obtained for composites loaded with laser SWCNTs compared with those including arc-purified CNTs. This seems a striking feature, taking into account that, according to SEM analysis, no significant differences were found within their degree of dispersion. Therefore, their enhanced mechanical performance should be attributed to a stronger interfacial adhesion or a better filler orientation. Moreover, the laser process leads to CNTs of the highest purity and quality (few defects, high crystallinity, low amorphous carbon content) and larger aspect ratio (>10 000) when compared with any other synthesis methods; these characteristics make them potentially more efficient for composite reinforcement [49]. Acid treatments, such as that used in this work to purify the arc grown SWCNTs, are known to shorten the CNTs and induce defects on their side walls, thus having detrimental effects on mechanical properties of the SWCNTs [50]. However, further experiments would be required to confirm the reasons for the differences observed among the composites tested. DMA analysis performed on samples with varying CNT loading showed a progressive enhancement in the storage modulus of the matrix upon incorporation of increasing amounts of SWCNTs. Thus, at room temperature, composites containing 0.1, 0.5 and 1 wt% laser SWCNTs increased $E'$ by approximately 15, 23 and 27%, respectively, whereas the increments for the same concentrations of these CNTs dispersed in PEI were 16, 28 and 35%. These data reveal a more linear growth of $E'$ with filler loading for the compatibilized samples. According to SEM observations, at very low SWCNT content, the nanotubes are uniformly dispersed in both types of samples. However, at higher concentrations, the tubes have a higher tendency to form small aggregates in the non-compatibilized nanocomposites,

and this is reflected in a smaller increase in their $E'$ values. A comprehensive study of the mechanical properties of these materials will be undertaken in the near future and reported elsewhere.

### *3.7. Electrical and thermal conductivity*

Thermally and electrically conductive polymer composites are widely used in the electronics and aerospace industries to dissipate heat and prevent the build up of static charge. However, fundamental research on these types of materials must be undertaken to understand more about the influence of the filler characteristics. The results from electrical and thermal conductivity measurements made at room temperature on PEEK/SWCNT nanocomposites with a different filler content are presented in figure 9. Pure PEEK is an insulating polymer ($\sigma < 10^{-13}$ S cm$^{-1}$) [51], and becomes electrically conductive upon the incorporation of CNTs. For PEEK/SWCNT nanocomposites, conductivity values increased dramatically up to $10^{-2}$ S cm$^{-1}$ (see figure 9(a)), due to the formation of effective electrical conductive paths in the polymer matrix. Such a magnitude of enhancement has only been reported in the literature for composites incorporating loosely entangled and uniformly distributed CNTs [52]. Thereby, our electrical measurements reveal a good dispersion of the filler within the PEEK matrix, in agreement with SEM observations. For each type of composite, no significant changes are observed with increasing CNT concentration, which suggests that the nanotube content is above the percolation threshold [52], and additional loading does not greatly reduce the resistance of the composite. Samples that include the compatibilizer show conductivity values about one order of magnitude lower than those without PEI. This could be explained by the fact that PEI is wrapped around the SWCNTs, which leads to a decrease in the number of contacts between the tubes, and hence a reduction in the electrical conductivity. Composites reinforced with laser grown SWCNTs exhibit ∼20% higher conductivity than those incorporating arc-purified CNTs, which is consistent with their greater improvement in the mechanical properties, attributed to the higher quality and lower defect content of this type of filler.

The room temperature thermal conductivities as a function of the CNT loading (figure 9(b)) display a similar behaviour to that observed from the electrical measurements. Nevertheless, in contrast to the orders of magnitude enhancement in electrical conductivity, the thermal conductivities of the composites show only a modest improvement in comparison to that of the pure polymer (0.23 W mK$^{-1}$). Furthermore, the changes in thermal conductivity with increasing filler loading are more significant. At 0.1, 0.5 and 1 wt% CNT content, the increase was about 40, 115 and 150%, respectively, for composites including laser grown SWCNTs, whereas for the corresponding compatibilized samples the increment was reduced to 23, 60 and 90%. Taking into account the exceptionally high thermal conductivity of SWCNTs (∼$10^3$ W mK$^{-1}$) [5], all the values cited above are considerably lower than predicted by the rule of mixing. This discrepancy could be attributed to the small thermal conductance of the nanotube–matrix interface [53]. With regard to the influence of the type of filler, it is confirmed, once again, that composites incorporating laser grown SWCNTs exhibit the highest values.

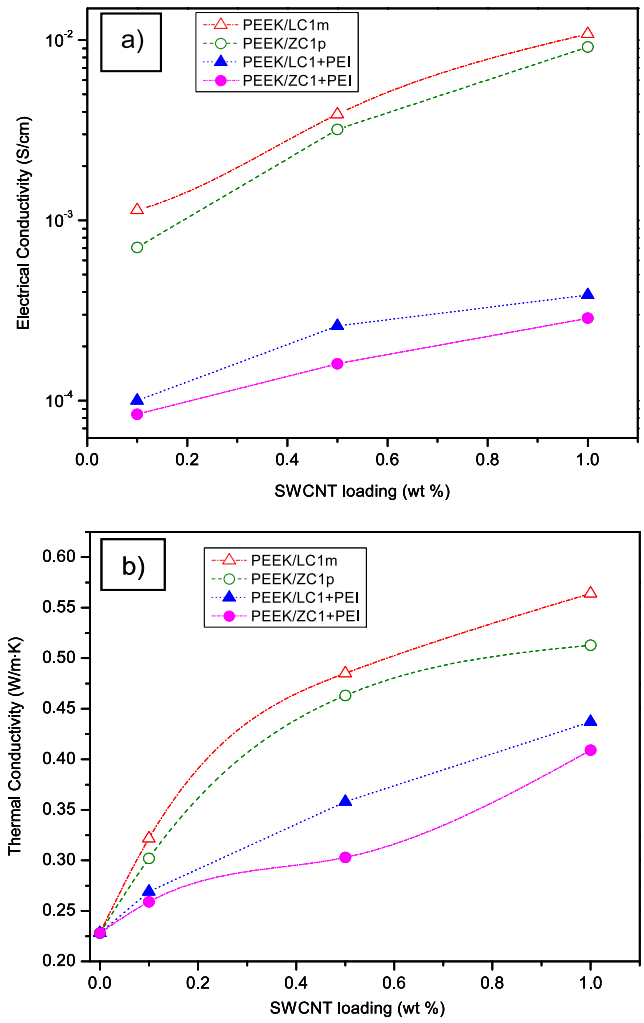


**Figure 9.** Room temperature DC volume conductivity (a) and thermal conductivity (b) for the different types of PEEK/SWCNT composites as a function of SWCNT loading.

## 4. Conclusions

In the present work, the morphology, thermal, electrical and dynamic mechanical properties of PEEK/SWCNT nanocomposites, at different CNT concentrations, have been investigated and compared with those modified with PEI as a compatibilizer. Morphological observations showed that the addition of the compatibilizer significantly reduced the size of the filler phase and improved their dispersion within the matrix. TGA thermograms revealed a substantial increase in the matrix degradation temperatures under dry air and nitrogen atmospheres upon the addition of SWCNTs; the compatibilizer maintains the level of thermal stability attained in the binary nanocomposites. Furthermore, over the whole composition range, higher decomposition

temperatures were observed for samples containing arc-purified SWCNTs. Compatibilized samples display lower crystallization temperatures and degrees of crystallinity, ascribed to the combination of a nanoconfinement effect and the incorporation of an amorphous polymer miscible with the matrix which perturbs its crystallization. Moreover, the analysis of the WAXS diffractograms showed similar effects in the crystallization data. The evolution of the long period $L$ with temperature indicates the existence of reorganization phenomena and improvement (i.e., perfection and thickening) of the PEEK crystals during the heating, maximized in the compatibilized nanocomposites, which exhibit lower $L$ values. DMA measurements indicate that the compatibilization leads to a significant enhancement in the storage modulus of the nanocomposites, due to an improved interfacial adhesion and stress transfer ability between the reinforcement and the matrix. Moreover, an increase in the glass transition temperatures of the samples is produced, due to the chain motion restriction imposed by their stronger interfacial interactions. For all the concentrations studied, an improved mechanical response was found in composites reinforced with laser grown SWCNTs. Samples including compatibilizer show electrical and thermal conductivity values lower than non-compatibilized composites; the wrapping of the PEI around the SWCNTs leads to a diminution in the number of contacts between the tubes, and consequently a reduction in the conductivity. Despite this decrease, their conductivity is far superior to that of the PEEK matrix, and sufficient to effectively dissipate heat and prevent the build up of static charge. Considering all the analyses performed, it can be concluded that these nanocomposites are effectively compatibilized with PEI, particularly at higher nanotube loading, where the enhancement in stiffness is more significant. This makes them interesting multifunctional materials for possible industrial applications.

## Acknowledgments

Financial support from a coordinated project between the National Research Council of Canada (NCR) and the Spanish National Research Council (CSIC) is gratefully acknowledged. Dr A Diez and Dr M Naffakh (I3PDR-6-02) would like to thank to Consejo Superior de Investigaciones Científicas (CSIC) for postdoctoral contracts. X-ray experiments were performed at the Soft Condensed Matter A2 beamline of the HASYLAB synchrotron (DESY–Hamburg, I-20080056 EC), supported by the European Commission. The authors would like to thank Dr S Funari for his technical assistance in the synchrotron experiments. The authors are also grateful to Dr A Johnston for providing the opportunity to perform conductivity measurements at the NRC Institute of Aerospace Research (Canada).

## References

[1] Thostenson E T, Ren Z and Chou T-W 2001 *Compos. Sci. Technol.* **61** 1899
[2] Xie X L, Mai Y-W and Zhouet X-P 2005 *Mater. Sci. Eng.* R **49** 89
[3] Liu T X, Phang I Y, Shen L, Chow S Y and Zhang W D 2004 *Macromolecules* **37** 7214
[4] Cadek M, Coleman J N, Barron V and Hedicke K 2002 *Appl. Phys. Lett.* **81** 739
[5] Raravikar N R, Schadler L S, Zhao Y P, Wei B Q and Ajayan P M 2005 *Chem. Mater* **17** 974
[6] Mangalgiri P D 1999 *Bull. Mater. Sci.* **22** 657
[7] Rueckes T, Kim K, Joselevich E, Tseng G Y, Cheung C-L and Lieber C M 2000 *Science* **289** 94
[8] Beland S 1990 *High Performance Thermoplastic Resins and their Composites* (New Jersey: Noyes Publications) p 136
[9] Pham J Q, Mitchell C A, Bahr J L and Tour J M 2003 *J. Polym. Sci. B: Polym. Phys.* **41** 3339
[10] Xie H, Liu B, Yuan Z, Shen J and Cheng R 2004 *J. Polym. Sci. B: Polym. Phys.* **42** 3701
[11] Kim J Y and Kim S H 2006 *J. Polym. Sci. B: Polym. Phys.* **44** 1062
[12] Barraza H J, Pompeo F, O'Rea E A and Resasco D E 2002 *Nano Lett.* **2** 797
[13] Tibbetts G G and McHugh J J 1999 *J. Mater. Res.* **14** 2871
[14] Gojny F and Schulte K 2004 *Compos. Sci. Technol.* **64** 2303
[15] Bafna S S, Sun T and Baird D G 1993 *Polymer* **34** 708
[16] Lee W C and DiBenedetto T 1993 *Polymer* **34** 684
[17] Zhang C-L, Feng L-F, Gu X-P, Hoppe S and Hu G-H 2007 *Polymer* **48** 5940
[18] Wills J M and Davis B D 1988 *Polym. Eng. Sci.* **28** 1416
[19] Searle O B and Pfeiffer R H 1985 *Polym. Eng. Sci.* **25** 474
[20] Hudson S D, Davis D and Lovinger A J 1992 *Macromolecules* **25** 1759
[21] Grevecoeur G and Groeninckx G 1991 *Macromolecules* **24** 1190
[22] Yano K, Usuki A, Okada A, Kurauchi T and Kamigaito O 1993 *J. Polym. Sci. Polym. Chem.* **31** 1942
[23] Jenkis M J 2001 *Polymer* **42** 1981
[24] Bicakci S and Cakmak M 2002 *Polymer* **43** 149
[25] Rath T, Kumar S, Mahaling R N, Mukherjee M and Das C K 2006 *Polym. Compos.* **27** 533
[26] Rath T, Kumar S, Mahaling R N, Khatua B B, Das C K and Yadaw S B 2008 *Mater. Sci. Eng.* A **490** 198
[27] Journet C, Maser W K, Bernier P, Loiseau A, Lamy de la Chapelle M, Lefrant S, Deniard P, Lee R and Fischer J E 1997 *Nature* **388** 756
[28] Blundell D J and Osborn B N 1983 *Polymer* **24** 953
[29] Elsner G, Riekel C and Zachmann H G 1985 *Adv. Polym. Sci.* **67** 1
[30] Ajayan P M, Schandler L S, Giannaris C and Rubio A 2000 *Adv. Mater.* **12** 750
[31] Pichaiyut S, Nakason C, Kaesaman A and Kiatkamjornwong S 2008 *Polym. Test.* **27** 566
[32] Shen H, Wang Y and Mai K 2008 *Thermochim. Acta* **483** 36
[33] Pang L S K, Saxby J D and Chatfield S P 1993 *J. Phys. Chem.* **97** 6941
[34] Kashiwagi T, Du F, Douglas J F, Winey K I, Harris R H and Shields J R 2005 *Nat. Mater.* **4** 928
[35] Li L, Li C Y, Ni C, Rong L and Hsiao B 2007 *Polymer* **48** 3452
[36] Jin J and Song M 2007 *Thermochim. Acta* **456** 25
[37] Naffakh M, Marco C, Gomez M A and Jímenez I 2008 *J. Phys. Chem.* B **112** 14819
[38] Datta J and Nandi A K 1996 *Polymer* **37** 5179
[39] Naffakh M, Gomez M A, Ellis G and Marco C 2003 *Polym. Int.* **52** 1876
[40] Sandler J, Werner P, Shaffer M S P, Demchuck V, Altstadt V and Windle A H 2002 *Composites* A **33** 1033
[41] Cser F 2000 *J. Appl. Polym. Sci.* **80** 2300
[42] Bark M, Schulze C and Zachmann H G 1990 *Polym. Prepr. (Am. Chem. Soc., Div. Polym. Chem.)* **31** 106
[43] Krueger K N and Zachmann H G 1993 *Macromolecules* **26** 5202

[44] Kumar S, Rath T, Mahaling R N, Reddy C S, Das C K, Pandey K N, Srivastava R B and Yadaw S B 2007 *Mater. Sci. Eng.* B **141** 61
[45] Cebe P, Chung S Y and Hong S D 1987 *J. Appl. Polym. Sci.* **33** 487
[46] Mehta A and Isayev A I 1991 *Polym. Eng. Sci.* **31** 963
[47] Goodwin A A and Simon G P 1997 *Polymer* **38** 2363
[48] Fox T G 1965 *Bull. Am. Phys. Soc.* **1** 123
[49] Coleman J N, Khan U, Blau W J and Gun'ko Y K 2006 *Carbon* **44** 1624
[50] Haskins R W, Maier R S, Ebeling R M, Marsh C P, Majure D L, Bednar A J, Welch C R and Barker B C 2007 *J. Chem. Phys.* **127** 74708
[51] Song L, Zhang H, Zhang Z and Xie S 2007 *Composites* A **38** 388
[52] Li J, Ma P C, Chow W S, To C K, Tang B Z and Kim J-K 2007 *Adv. Funct. Mater.* **17** 3207
[53] Moniruzzaman M and Karen I W 2006 *Macromolecules* **39** 5202